Atomic-Scale Clarification of Structural Transition of MoS_2 upon Sodium Intercalation

Xuefeng Wang,[†] Xi Shen,[‡] Zhaoxiang Wang,[*,†] Richeng Yu,[*,‡] and Liquan Chen[†]

[†]Key Laboratory for Renewable Energy, Chinese Academy of Sciences, Beijing Key Laboratory for New Energy Materials and Devices, Beijing National Laboratory for Condensed Matter Physics, Institute of Physics, Chinese Academy of Sciences, P.O. Box 603, Beijing 100190, China and [‡]Laboratory for Advanced Materials & Electron Microscopy, Beijing National Laboratory for Condensed Matter Physics, Institute of Physics, Chinese Academy of Sciences, P.O. Box 603, Beijing 100190, China

ABSTRACT Two-dimensional (2D) transition-metal dichalcogenides hold enormous potential for applications in electronic and optoelectronic devices. Their distinctive electronic and chemical properties are closely related to the structure and intercalation chemistry. Herein, the controversial phase transition from semiconductive 2H to metallic 1T phase and occupancy of the intercalated sodium (Na) upon electrochemical Na intercalation into MoS_2 are clarified at the atomic scale by aberration-corrected scanning transmission electron microscope. In addition, a series of other complicated phase transitions along with lattice distortion, structural modulation, and even irreversible structural decomposition are recognized in MoS_2 depending on the content of Na ion intercalation. It is shown that $x = 1.5$ in Na_xMoS_2 is a critical point for the reversibility of the structural evolution. Our findings enrich the understanding of the phase transitions and intercalation chemistry of the MoS_2 and shed light on future material design and applications.

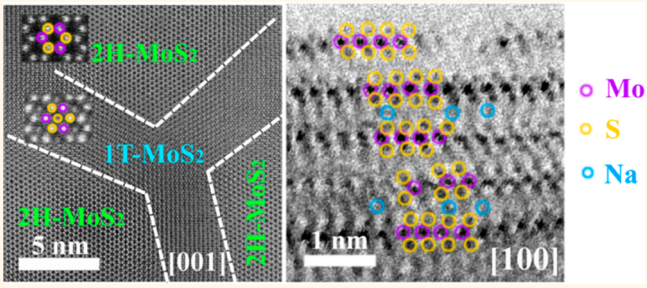

KEYWORDS: layered compounds · molybdenum disulfide · intercalation · phase transition · sodium ion battery

Two-dimensional transition metal dichalcogenides MX_2 (M = Mo, W, Ti, *etc.*, ; X = S, Se, Te) are composed of hexagonally coordinated X−M−X atomic slabs.[1] The parallel and neighboring slabs are interconnected with weak van der Waals force. The large space between the slabs and their electrostatic stabilization of the negatively charged S^{2-} ions permit intercalation of guest atoms such as alkali metals and even molecules therein, and intercalation compounds are formed.[2] Intercalation reaction and the intercalation compounds have become the base of science and technology for energy conversion and storage[3−5] as well as two-dimensional nanosheet preparation.[6,7] Better understanding of the structural evolution and intercalation chemistry of the MX_2 is beneficial for material design and applications.

As a typical metal dichalcogenide and direct-bandgap material, molybdenum disulfide (MoS_2) shows great application potentials in electrical and optoelectronic devices.[8−11] Its electronic properties are closely dependent on its crystalline structure;[12] the 2H-MoS_2 phase has been known to be semiconductive while the 1T-MoS_2 phase is metallic. The metastable 1T phase can be obtained by intercalation of alkali metals (Li, Na, K) into 2H-MoS_2[13] but unstable in air and easily transformed back to 2H phase at room temperature.[14] The transition from 2H-MoS_2 to 1T-MoS_2 is supposed to involve a glide of intralayer atomic planes[15] but has never been confirmed/observed at the atomic scale.

Lithium (Li) ion intercalation in 2H-MoS_2 has been widely explored for Li-ion batteries[16] and chemically/electrochemically exfoliated preparation of single-layer MoS_2 nanosheets.[17] This process is believed to experience a series of structural transformations, including 2H- to 1T-MoS_2 phase transition (Li_xMoS_2, $0.5 < x < 1$).[18−21] However, the structural evolution of MoS_2, especially the intermediate phases such as 1T-MoS_2 and the occupancy of the Li atoms in it, is still not clear. Clearly, intercalation of larger

* Address correspondence to zxwang@iphy.ac.cn, rcyu@aphy.iphy.ac.cn.

Received for review August 9, 2014 and accepted November 2, 2014.

Published online November 02, 2014
10.1021/nn505501v

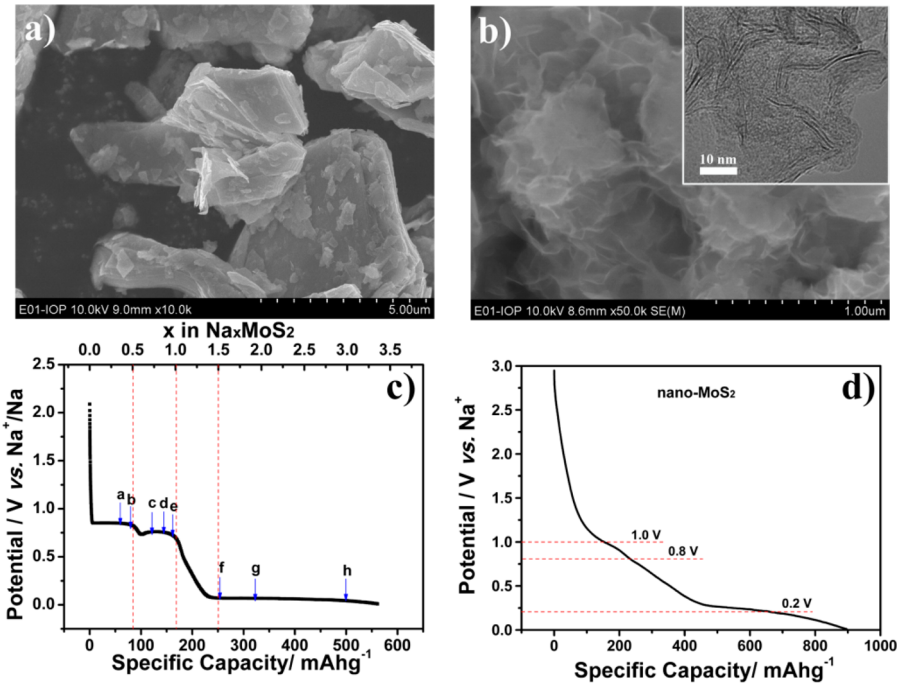

Figure 1. Scanning electron microscopic (SEM) images (a and b) and initial discharge potential profile of Na intercalation (c and d) in commercial (a and c) and home-prepared nanoscaled MoS_2 (b and d) (the mass of active material is *ca.* 5.0 mg cm^{-2} on each electrode sheet). The inset in panel b shows the transmission electron microscopic (TEM) image of nano-MoS_2. The top axis of panel c shows the corresponding content of the Na ions intercalated in MoS_2 under the assumption that all the Na ions are used for intercalation in MoS_2. This has been determined with calculations based on the conservation of charge and confirmed with the inductively coupled plasma-optical emission spectroscopic (ICP) results of the cycled electrodes. Three clear discharge plateaus (at *ca.* 0.85 , 0.75, and 0.06 V) and two slopes (0.85−0.75 and 0.75−0.06 V) can be well recognized in the discharge profile of commercial MoS_2 (c), corresponding to a series of structural changes.

guest ions, such as Na, will lead to more apparent structural changes in MoS_2 and make the observation easier.

It was difficult to determine the stoichiometry of Na_xMoS_2 intercalation compounds by traditional chemical methods due to uncontrollable content of intercalated Na and disordered MoS_2 structure[13,22,23] and impossible to recognize the occupancy of Na_xMoS_2 at the atomic level in the past. In this work, controlled contents of Na ions are electrochemically intercalated into MoS_2 and the structural evolution of MoS_2 is monitored by *in situ* and *ex situ* techniques. The phase transition from 2H-MoS_2 to 1T-MoS_2 and occupation of Na ions are clarified at the atomic scale. In addition, more phase transition features of MoS_2 are observed during extensive Na insertion and extraction as well as partially staging intercalation. Our findings shed light on the understanding of the intercalation chemistry of the MoS_2 and benefit for future material design and applications in semiconductors and energy conversion and storage devices, *e.g.*, sodium ion batteries.[24−28]

RESULTS

Both commercial (Figure 1a) and home-prepared nanoscaled (Figure 1b) MoS_2 are used in this work. The intercalation process of Na ions (discharge) in commercial MoS_2 can be easily controlled by tuning the cutoff discharge (Na intercalation) potential or time in a galvanostatic mode (the capacity or content of the Na ions inserted in MoS_2 is directly proportional to the discharge time). Figure 1c shows the discharge potential profile of commercial MoS_2 between 3.00 and 0.01 V *vs* Na^+/Na. Three clear discharge plateaus (at *ca.* 0.85, 0.75, and 0.06 V, respectively) and two slopes (0.85−0.75 and 0.75−0.06 V) can be well recognized in the discharge profile of commercial MoS_2, corresponding to a series of structural changes. These plateaus become vague in the discharge profile of nano-MoS_2 due to its low crystallinity (Figure 1d). Therefore, commercial MoS_2 is used for phases monitoring, while the home-prepared few-layered nano-MoS_2 is favorable for atomic observation of Na occupancy.

In situ X-ray diffraction (XRD; Figure 2a) is performed on a MoS_2/Na cell cycled between 0.01 and 3.00 V at a current density of 20 mA g^{-1}. To receive sufficiently strong XRD signals, a thick commercial MoS_2 electrode (mass of active material *ca.* 23.0 mg cm^{-2} on the electrode sheet) is prepared, which leads to slight polarization of the cell and disappearance of the lower plateau. The patterns clearly show that the structural changes of MoS_2 below 1.00 V are two-phase transitions, from 2H-MoS_2 ($2\theta_{(002)} = 14.38°$; $a = 3.16$ Å and $c = 12.29$ Å) to 2H−$Na_{0.5}MoS_2$ ($2\theta_{(002)} = 11.82°$; $a = 3.21$ Å and $c = 15.06$ Å) on the upper plateau (0.85 V), and from 2H−$Na_{0.5}MoS_2$ to 1T-$NaMoS_2$ ($2\theta_{(002)} = 12.42°$; $a = 3.11$ Å and $c = 14.29$ Å) on the middle plateau (0.75 V),

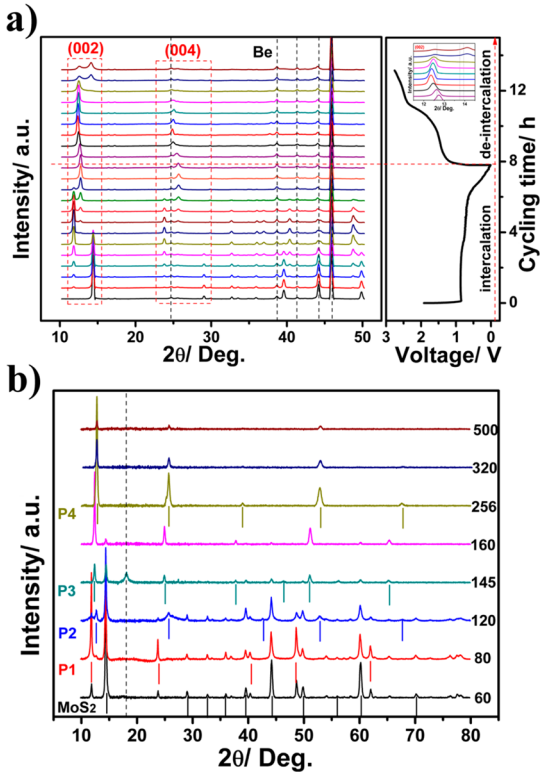

Figure 2. *In situ* (a) and *ex situ* (b) XRD patterns of commercial MoS_2 containing different contents of electrochemically intercalated Na ions. The inset of the potential profile in (a) is for the selected XRD patterns during Na deintercalation. The numbers on the right of (b) are for the capacity (mAh g^{-1}) of intercalated Na in MoS_2 as shown in Figure 1c. The Na ion intercalation leads to a series of two-phase structural transitions. The new phases are denoted as P1 to P4, corresponding to 2H-$Na_{0.5}MoS_2$ (P1; c = 15.06 Å and a = 3.21 Å), 1T-$Na_{0.5}MoS_2$ (P2; c = 13.97 Å and a = 3.06 Å), 1T-$NaMoS_2$ (P3; c = 14.29 Å and a = 3.11 Å) and Na_xS (P4; c = 13.97 Å and a = 3.43 Å), respectively, and their diffraction peaks are labeled by short vertical.

respectively. Insertion of more Na ions (Na_xMoS_2, 1.0 < x < 1.5) does not lead to any detectable structural changes after that.

The subsequent deintercalation process begins as a solid-solution reaction. The prominent diffraction peaks, the (002) diffraction, for example, shift toward the lower 2θ angles until 1.50 V before going back to higher 2θ angles continuously; no new diffractions are observed in this process. Close to the end of deintercalation (above 2.50 V), a two-phase transition occurs from 1T-$Na_{0.5}MoS_2$ to 1T-MoS_2 ($2\theta_{(002)}$ = 14.07°) rather than the starting 2H-MoS_2 ($2\theta_{(002)}$ = 14.38°). It seems that x = 1.5 in Na_xMoS_2 is a critical point for the reversibility of the structural evolution. The structure of MoS_2 can be partially recovered at the end of deintercalation (the top 2 lines of Figure 2a and Supporting Information Figure S1) if less than 1.5 Na is intercalated (before the lower plateau appears in Figure 1c).

As the time interval between every two XRD patterns is long (40 min) and the current density (20 mA g^{-1}) is high in the above *in situ* test, some important information might have been missed between the recorded patterns. *Ex situ* XRD experiment (Figure 2b) is performed from states *a* to *g* in Figure 1c (samples are denoted as Cell-60, Cell-80, *etc.*; the number is for the corresponding specific capacity). The *ex situ* XRD patterns agree well with the *in situ* patterns. It confirms the presence of the above-mentioned two-phase reactions. In addition, the 1T-$Na_{0.5}MoS_2$ phase ($2\theta_{(002)}$ = 12.68°; a = 3.06 Å and c = 13.97 Å) can be recognized in Cell-120 sample (a point on the upper slope between 0.85 and 0.75 V). As more Na ions are inserted into MoS_2 for the *ex situ* XRD samples, decomposition of MoS_2 can be detected in sample Cell-256 (Figure 2b). One of the decomposition products is hexagonal Na_xS ($2\theta_{(002)}$ = 12.80°; a = 3.43 Å and c = 13.91 Å). The other decomposition product is recognized to be metallic Mo according to the X-ray photoelectron spectrum (XPS; Figure 4a) though it is not detected by XRD due to its nanoscale dispersion. Insertion of more Na ions does not lead to the appearance of any new phases until the end of discharge (a total of 500 mAh g^{-1}, including Na ions consumed on the electrolyte decomposition and other side reactions). Once Na_xMoS_2 is completely converted to metallic Mo and Na_xS, no MoS_2 can be obtained up to 3.0 V during Na deintercalation (Supporting Information Figure S2).

The structural evolutions of MoS_2, especially its phase transition from 2H- to 1T-MoS_2 and the occupancy of the Na ions during the intercalation, are recognized at the atomic scale by advanced aberration-corrected scanning transmission electron microscopy (STEM) (Figure 3). Commercial MoS_2 is favorable for observation along the *c* axis rather than along the *a* or *b* axis due to its condensed lamellar stacking structure and large particle. The 2H-MoS_2 (Figure 3a,e) shows a hexagonal lattice with 3-fold symmetry and the atomic stacking sequence (S−Mo−S) of ABA, while the 1T-MoS_2 shows atomic stacking sequence (S−Mo−S′) of ABC where the bottom S′ plane occupies the hollow center of 2H hexagonal lattice (Figure 5).[29] These two phases can easily convert to each other by a glide of the intralayer atomic planes, which involves a transversal displacement of one of the sulfur planes.[15] The high-angle annular dark field (HAADF) image of 1T-MoS_2 along [001] zone axis (Figure 3c) shows that another S atom appears and occupies the hollow center of the hexagonal lattice of 2H-MoS_2. It should be noted that the selected area electron diffraction (SAED) pattern along [001] zone axis of 1T phase (Figure 3g) is the same as that of 2H phase (Figure 3e). Figure 3b shows a coexistence region of these two phases, where 1T-MoS_2 is squeezed by 2H-MoS_2 and the corresponding SAED pattern is shown in Figure 3f. Therefore, the phase transition from 2H-MoS_2 to 1T-MoS_2 induced by Na intercalation can be deduced as follows. First, the in-plane strain deduced by Na intercalation promotes the shrinkage of the Mo−Mo distance and the nucleation of 1T-MoS_2 at the boundary. Then the boundaries migrate to enlarge the region of

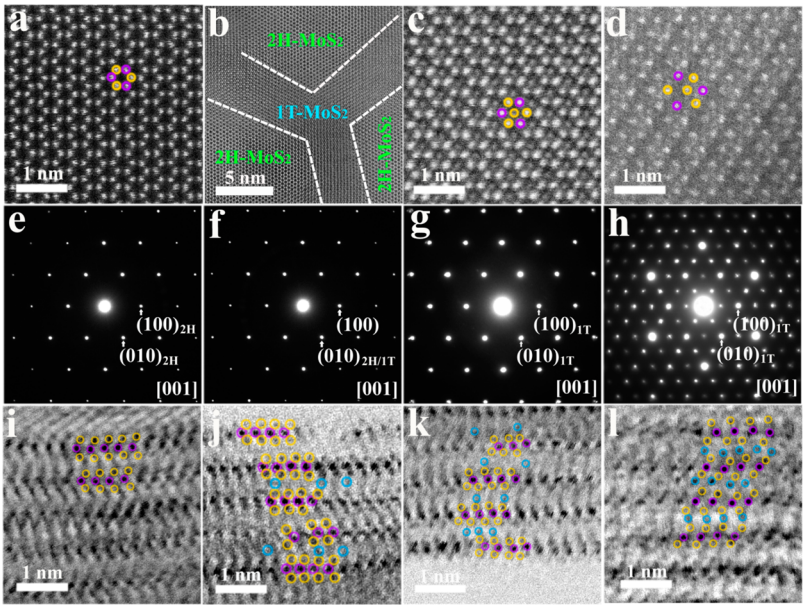

Figure 3. High-angle annular dark-field (HAADF), and selected area electron diffraction (SAED) images of commercial MoS_2 in Cell-60 (a and e), Cell-80 (b and f), Cell-160 (c and g), and Cell-256 (d and h) along the [001] zone axis and the annular bright-field (ABF) images of as-prepared nano-MoS_2 (i) with cutoff at 1.0 V (j), 0.8 V (k), and 0.2 V (l) along the [100] zone axis. The purple, yellow, and blue circles are overlaid in the image for Mo, S, and Na atoms, respectively. The SAED patterns are indexed according to the MoS_2 structure. The Na ion intercalation leads to phase transitions from 2H (a and e) to 1T (c and g) phase then lattice distortion (d) and a 2×2 modulated structure (h). The Na ions first intercalate in every other interlayer (b), then fill the other interlayers (c) before former interlayers are fully occupied and finally fulfill all interlayers (d) of MoS_2 (a).

1T-MoS_2. This process is completed before one Na ion is intercalated into each formula of MoS_2 (Figure 3c). Note that the angle of two neighboring boundaries is about 120°, 1T-MoS_2 is more likely to grow along some specific lattice planes, such as (100). Intercalation of more Na ions leads to lattice distortion and a modulated structure, including 2×2 (Figure 3d,h) and 4×4 (Supporting Information Figure S3), probably due to the formation of Mo zigzag-chain clusters.[30]

Direct observation of the Na occupancy in MoS_2 is carried out by annular bright field (ABF) imaging technique along its *a*/*b* axis. Figure 3i exhibits S−Mo−S zigzag-chain arrangement of as-prepared few-layered 2H-MoS_2 (Figure 1b for its morphology and Figure 1d for its intercalation potential profile). Upon discharge, the Na ions are first intercalated into every other interlayer of MoS_2 while the other interlayers keep empty (Figure 3j). Before those layers are fully occupied (Figure 3k), the Na ions begin to fill the empty layers when more Na ions are intercalated. This is similar to the *staging* feature of lithium intercalation in graphite[31] but is different from the graphite case because the Na intercalation in MoS_2 is not a fully staged one. Meanwhile, the sulfur planes glide along an intralayer atomic plane to form 1T-MoS_2, resulting in a straight chain of S−Mo−S (Figure 3k). The successively intercalated Na ions fulfill all the residual empty sites within the interlayer of MoS_2 (Figure 3*l*).

This intercalation mechanism is further confirmed by comparing the average layer spacing in above ABF images (Supporting Information Figure S4). The average layer spacing of initial nano-MoS_2 is about 0.61−0.68 nm due to the distorted nanosheet structure and Na ion intercalations increase the spacing to 0.72 nm, in accordance with the above XRD results. The staggered spacing between 0.68 and 0.72 nm in Figure 3j and the similar spacing about 0.72 nm in Figure 3l suggest that the Na ions are first intercalated in every other interlayer and then fulfill all the interlayers of MoS_2. It is worth pointing out that higher quality STEM images cannot be obtained because the samples are thick and distorted and the presence of the solid electrolyte interphase layers (a deposition of the electrolyte decomposition below 0.7 V *vs* Na^+/Na) disturbs the observation.

The XPS (Figure 4a) and Raman (Figure 4b) spectra indicate that Na_xMoS_2 is decomposed to Na_xS (Figure 2b) and metallic Mo (Figure 4a) when more than 1.5 Na ions per formula of MoS_2 are intercalated. As shown in Figure 4a, the intercalated Na ions donate electrons to MoS_2, resulting in the blue shifting of the Mo 3d peaks. The energy difference between Cell-60 and Cell-80 is about 0.8 eV, in accordance with the reported value when the 2H to 1T phase transition happens.[21,23] Furthermore, a new Mo $3d_{3/2}$ peak appears at 230.5 eV for the formation of metallic Mo in sample Cell-145. As the intercalation goes further (Cell-256), only metallic Mo can be detected. Meanwhile, the two prominent peaks of MoS_2, at 383 cm^{-1} for the E^1_{2g} mode and at 408 cm^{-1} for the A_{1g} mode,[32] disappear in Cell-256 (Figure 4b), implying the breakdown of S−Mo−S bond. This is due to the enhanced of S−Na bond and weakened of S−Mo bond with Na ion intercalations. However, no

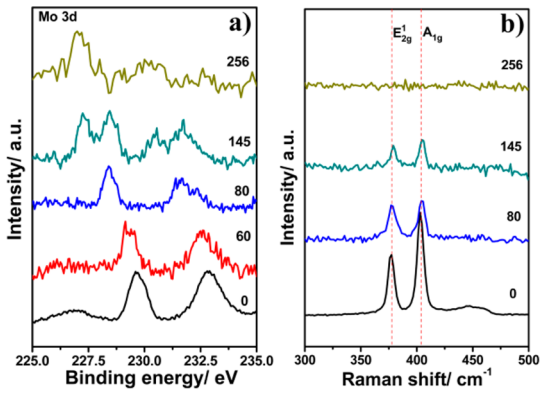

Figure 4. XPS spectra (a) of Mo 3d and the Raman spectra (b) at various Na intercalation stages in MoS_2. A new Mo $3d_{3/2}$ peak appears at 230.5 eV for the formation of metallic Mo in sample Cell-145 (a). The two prominent peaks of MoS_2, at 383 cm^{-1} for the E^1_{2g} mode and at 408 cm^{-1} for the A_{1g} mode, disappear in Cell-256 (b), implying the breakdown of S−Mo−S bond.

Mo clusters are observed by STEM or XRD until very low potentials (0.01 V). Therefore, the metallic Mo in the matrix of decomposed MoS_2 is believed to be well-dispersed at the nanoscale level, similar to the distribution of the electrochemically converted metallic nickel (Ni) from nickel oxide (NiO),[33] or metallic Mo from MoS_2,[19,20] upon Li-ion insertion.

DISCUSSIONS

A combination of the above results demonstrates that MoS_2 experiences a series of two-phase transitions upon Na insertion, the phases including 2H-MoS_2 (c = 12.29 Å and a = 3.16 Å), 2H−$Na_{0.5}MoS_2$ (P1; c = 15.06 Å and a = 3.21 Å), 1T-$Na_{0.5}MoS_2$ (P2; c = 13.97 Å and a = 3.06 Å), 1T-$NaMoS_2$ (P3; c = 14.29 Å and a = 3.11 Å) and Na_xS (P4; c = 13.97 Å and a = 3.43 Å). The Na ions are first intercalated in every other interlayer of MoS_2 to form hexagonal $Na_{0.5}MoS_2$, corresponding to the upper plateau at *ca.* 0.85 V. Before these interlayers are fully occupied, the Na ions begin to fill the other interlayers between the S−Mo−S slabs. The large strain and unfavorable energy induce glide of the sulfur plane along an intralayer atomic plane and phase transition from 2H- to 1T-MoS_2, where the Mo atom-coordination transfers from trigonal to octahedral and its schematic diagram is shown in Figure 5.

With further Na ion intercalation, all the interlayers are fulfilled, leading to lattice distortion and 2 × 2 structural modulation in the middle voltage slope. If the intercalation is stopped here or earlier, the Na ion intercalation will remain topologic and the structure of MoS_2 can be partially recovered after most of the intercalated Na ions are deintercalated. Then the subsequent Na-ion intercalation is similar to the before, and two apparent biphasic transitions occur during continual intercalation, as shown in the *in situ* XRD patterns for the Na-ion reintercalation (Supporting Information Figure S5). However, the Na_xMoS_2 will be decomposed to metallic Mo and hexagonal Na_xS at the lower plateau when the intercalation is further performed. The metallic Mo is well-dispersed at the atomic scale. A 4 × 4 modulated structure is formed apparently (Supporting Information Figure S3). In this case, the structure of MoS_2 cannot be restored up to 3.0 V and only Na_xS participates in the subsequent reaction. These different subsequent processes lead to the distinctive potential profile in the following cycles (Supporting Information Figure S6) and their different electrochemical performances with different cutoff voltage will be illustrated in our further paper.

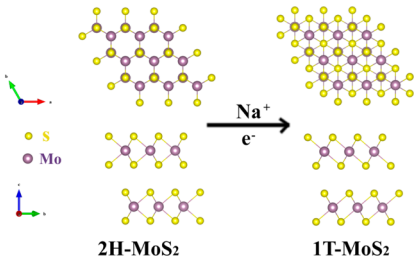

Figure 5. Schematic diagram for phase transition from 2H-MoS_2 to 1T-MoS_2. The 2H-MoS_2 shows hexagonal lattice with 3-fold symmetry and the atomic stacking sequence (S−Mo−S) of ABA while the 1T-MoS_2 shows atomic stacking sequence (S−Mo−S′) of ABC where the bottom S′ plane occupies the hollow center of 2H hexagonal lattice.

CONCLUSIONS

In summary, intercalation and deintercalation of Na ions are electrochemically controlled in/from the interlayers of MoS_2. The Na ion intercalation leads to a series of two-phase structural transitions. The phase transition from 2H-MoS_2 to 1T-MoS_2 is confirmed and described at the atomic scale. The intercalation process is partially staged. Depending on the depth of intercalation, the structure of MoS_2 can be partially recovered (to 1T-MoS_2) if less than 1.5 Na ions per formula of MoS_2 are intercalated. However, its structure cannot be restored once it is decomposed to Na_xS and metallic Mo. The critical point for the reversibility of structural evolution is $x \sim 1.5$ in Na_xMoS_2. Our findings enrich the understanding of the intercalation chemistry of the MoS_2 and benefit for future material design and applications in semiconductors and energy conversion and storage devices, *e.g.*, sodium ion batteries.

EXPERIMENTAL SECTION

All the chemicals are of analytical grade and used as received without further purification. The nano-MoS_2 is prepared by hydrothermal treatment of Na_2MoO_4 and NH_2CSNH_2 mixture at 200 °C for 12 h. The working electrode is prepared by casting a slurry of commercial MoS_2 (Alfa, > 99% in purity), multiwall

carbon nanotube (XF Nano; inter radius is 10−20 nm and length is 10−30 μm) and polyvinylidenefluoride (PVDF) in *N*-methyl-2-pyrrolidone (NMP) at a weight ratio of 75:15:10 on a clean Cu current collector.[34] In an Ar-filled glovebox, button-type test cells are assembled with Na foil as the counter electrode, glass fiber as the separator, and 1 mol L^{-1} $NaClO_4$ dissolved in a mixture of ethylene carbonate (EC) and diethyl carbonate (DEC) (4:6 in volume) as the electrolyte.

The electrochemical Na ions intercalation into MoS_2 and the performance evaluation of MoS_2 were carried out on a Land BT2000 battery tester (Wuhan, China) at room temperature. The cyclic voltammetry (CV) was recorded on a CHI600D electrochemical workstation (Shanghai, China) at a scan rate of 0.05 mV s^{-1}. The electrode sheets for *ex situ* characterization are obtained by rinsing the cycled electrode sheets with DEC, drying them in a vacuum mini-chamber of the glovebox, and finally transferring into the vacuum chamber of the instrument or testing in an airtight container.

Aberration-corrected scanning transmission electron microscopy (STEM) experiments are performed on a JEOL ARM200F transmission electron microscope equipped with a CEOS probe aberration corrector. The available spatial resolution of the STEM microscope is 75 pm at a collection semiangle of 21−25 mrad. Prior to STEM measurements, samples from cycled electrodes are dispersed in DEC and deposited on a carbon film coated copper grid. The Raman spectra were recorded on a Renishaw Via-Reflex spectrometer (532 nm radiation) with a resolution of 2 cm^{-1}. The X-ray photoelectron spectra (XPS) are recorded on an Escalab 25° XPS spectrometer (PerkinElmer Co). The spectrum is calibrated with C 1s (284.8 eV). All the *ex situ* tests are conducted in vacuum and under protection of Ar upon sample transfer.

The *in situ* X-ray diffraction (XRD) signals are collected on an X'Pert Pro MPD X-ray diffractometer (D8 Advance with a LynxEye_XEdetector, Bruker) with Cu Kα1 radiation (λ = 1.5405 Å) and metal beryllium (Be) as the window of a specially designed electrochemical cell. Polyvinylidenefluoride (PVDF) is used as the binder of the current collector free electrode. The positions of the diffractions were calibrated with that of the Be window material.

Conflict of Interest: The authors declare no competing financial interest.

Acknowledgment. This work was financially supported by the National Natural Science Foundation of China (NSFC No. 51372268) and the National 973 Program of China (Grant Nos. 2015CB251100 and 2012CB932302).

Supporting Information Available: Ex situ XRD patterns of MoS_2 at various deintercalation states from 0.2 and to 3.0 V (Figure S1); *ex situ* XRD patterns of Na deintercalated MoS_2 (Figure S2); selected area electron diffraction (SAED) pattern (Figure S3); the average layer spacing of the as-prepared nano-MoS_2 (Figure 3i) with cutoff at 1.0 V (Figure 3j), 0.8 V (Figure 3k) and 0.2 V (Figure 3l) (Figure S4); *in situ* XRD pattern of Na intercalation in the second cycle of 0.2−3.0 V (Figure S5) and potential profiles of electrode with different cutoff voltage (Figure S6). This material is available free of charge *via* the Internet at http://pubs.acs.org.

REFERENCES AND NOTES

1. Chhowalla, M.; Shin, H. S.; Eda, G.; Li, L.-J.; Loh, K. P.; Zhang, H. The Chemistry of Two-Dimensional Layered Transition Metal Dichalcogenide Nanosheets. *Nat. Chem.* **2013**, *5*, 263–275.
2. Benavente, E.; Santa Ana, M. A.; Mendizábal, F.; González, G. Intercalation Chemistry of Molybdenum Disulfide. *Coord. Chem. Rev.* **2002**, *224*, 87–109.
3. Etacheri, V.; Marom, R.; Elazari, R.; Salitra, G.; Aurbach, D. Challenges in the Development of Advanced Li-Ion Batteries: A Review. *Energy Environ. Sci.* **2011**, *4*, 3243–3262.
4. Goodenough, J. B.; Kim, Y. Challenges for Rechargeable Li Batteries. *Chem. Mater.* **2009**, *22*, 587–603.
5. Gao, M.-R.; Xu, Y.-F.; Jiang, J.; Yu, S.-H. Nanostructured Metal Chalcogenides: Synthesis, Modification, and Applications in Energy Conversion and Storage Devices. *Chem. Soc. Rev.* **2013**, *42*, 2986–3017.
6. Zeng, Z.; Yin, Z.; Huang, X.; Li, H.; He, Q.; Lu, G.; Boey, F.; Zhang, H. Single-Layer Semiconducting Nanosheets: High-Yield Preparation and Device Fabrication. *Angew. Chem., Int. Ed.* **2011**, *50*, 11093–11097.
7. Zeng, Z.; Sun, T.; Zhu, J.; Huang, X.; Yin, Z.; Lu, G.; Fan, Z.; Yan, Q.; Hng, H. H.; Zhang, H. An Effective Method for the Fabrication of Few-Layer-Thick Inorganic Nanosheets. *Angew. Chem., Int. Ed.* **2012**, *51*, 9052–9056.
8. Wang, Q. H.; Kalantar-Zadeh, K.; Kis, A.; Coleman, J. N.; Strano, M. S. Electronics and Optoelectronics of Two-Dimensional Transition Metal Dichalcogenides. *Nat. Nanotechnol.* **2012**, *7*, 699–712.
9. Huang, X.; Zeng, Z.; Zhang, H. Metal Dichalcogenide Nanosheets: Preparation, Properties and Applications. *Chem. Soc. Rev.* **2013**, *42*, 1934–1946.
10. Yin, Z.; Li, H.; Li, H.; Jiang, L.; Shi, Y.; Sun, Y.; Lu, G.; Zhang, Q.; Chen, X.; Zhang, H. Single-Layer MoS_2 Phototransistors. *ACS Nano* **2012**, *6*, 74–80.
11. Huang, X.; Tan, C.; Yin, Z.; Zhang, H. 25th Anniversary Article: Hybrid Nanostructures Based on Two-Dimensional Nanomaterials. *Adv. Mater.* **2014**, *26*, 2185–2204.
12. Mattheiss, L. Band Structures of Transition-Metal-Dichalcogenide Layer Compounds. *Phys. Rev. B* **1973**, *8*, 3719–3740.
13. Somoano, R. B.; Hadek, V.; Rembaum, A. Alkali Metal Intercalates of Molybdenum Disulfide. *J. Chem. Phys.* **1973**, *58*, 697–701.
14. Enyashin, A. N.; Yadgarov, L.; Houben, L.; Popov, I.; Weidenbach, M.; Tenne, R.; Bar-Sadan, M.; Seifert, G. New Route for Stabilization of 1T-WS_2 and MoS_2 Phases. *J. Phys. Chem. C* **2011**, *115*, 24586–24591.
15. Lin, Y. C.; Dumcenco, D. O.; Huang, Y. S.; Suenaga, K. Atomic Mechanism of the Semiconducting-to-Metallic Phase Transition in Single-Layered MoS_2. *Nat. Nanotechnol.* **2014**, *9*, 391–396.
16. Xiao, J.; Choi, D.; Cosimbescu, L.; Koech, P.; Liu, J.; Lemmon, J. P. Exfoliated MoS_2 Nanocomposite as an Anode Material for Lithium Ion Batteries. *Chem. Mater.* **2010**, *22*, 4522–4524.
17. Li, H.; Wu, J.; Yin, Z.; Zhang, H. Preparation and Applications of Mechanically Exfoliated Single-Layer and Multilayer MoS_2 and WSe_2 Nanosheets. *Acc. Chem. Res.* **2014**, *47*, 1067–1075.
18. Chang, K.; Geng, D.; Li, X.; Yang, J.; Tang, Y.; Cai, M.; Li, R.; Sun, X. Ultrathin MoS_2/Nitrogen-Doped Graphene Nanosheets with Highly Reversible Lithium Storage. *Adv. Energy Mater.* **2013**, *3*, 839–844.
19. Fang, X. P.; Hua, C. X.; Guo, X. W.; Hu, Y. S.; Wang, Z. X.; Gao, X. P.; Wu, F.; Wang, J. Z.; Chen, L. Q. Lithium Storage in Commercial MoS_2 in Different Potential Ranges. *Electrochim. Acta* **2012**, *81*, 155–160.
20. Stephenson, T.; Li, Z.; Olsen, B.; Mitlin, D. Lithium Ion Battery Applications of Molybdenum Disulfide (MoS_2) Nanocomposites. *Energy Environ. Sci.* **2014**, *7*, 209–231.
21. Wang, H.; Lu, Z.; Xu, S.; Kong, D.; Cha, J. J.; Zheng, G.; Hsu, P.-C.; Yan, K.; Bradshaw, D.; Cui, Y.; *et al.* Electrochemical Tuning of Vertically Aligned MoS_2 Nanofilms and Its Application in Improving Hydrogen Evolution Reaction. *Proc. Natl. Acad. Sci. U.S.A.* **2013**, *110*, 19701–19706.
22. Zak, A.; Feldman, Y.; Lyakhovitskaya, V.; Leitus, G.; Popovitz-Biro, R.; Wachtel, E.; Cohen, H.; Reich, S.; Tenne, R. Alkali Metal Intercalated Fullerene-Like MS_2 (M = W, Mo) Nanoparticles and Their Properties. *J. Am. Chem. Soc.* **2002**, *124*, 4747–4758.
23. Zheng, J.; Zhang, H.; Dong, S.; Liu, Y.; Nai, C. T.; Shin, H. S.; Jeong, H. Y.; Liu, B.; Loh, K. P. High Yield Exfoliation of Two-Dimensional Chalcogenides Using Sodium Naphthalenide. *Nat. Commun.* **2014**, *5*, 2995–3001.
24. Mortazavi, M.; Wang, C.; Deng, J.; Shenoy, V. B.; Medhekar, N. V. Ab Initio Characterization of Layered MoS_2 as Anode for Sodium-Ion Batteries. *J. Power Sources* **2014**, *268*, 279–286.
25. Bang, G. S.; Nam, K. W.; Kim, J. Y.; Shin, J.; Choi, J. W.; Choi, S.-Y. Effective Liquid-Phase Exfoliation and Sodium Ion Battery Application of MoS_2 Nanosheets. *ACS Appl. Mater. Interfaces* **2014**, *6*, 7084–7089.

26. Wang, Y.; Seng, k.; chou, s.; Wexler, D.; Guo, Z.; Liu, H.; Dou, S. X. Reversible Sodium Storage *via* Conversion Reaction in MoS_2/C Composite. *Chem. Commun.* **2014**, *50*, 10730–10733.
27. David, L.; Bhandavat, R.; Singh, G. MoS_2/Graphene Composite Paper for Sodium-Ion Battery Electrodes. *ACS Nano* **2014**, *8*, 1759–1770.
28. Wang, J.; Luo, C.; Gao, T.; Langrock, A.; Mignerey, A. C.; Wang, C. An Advanced MoS_2/Carbon Anode for High-Performance Sodium-Ion Batteries. *Small* **2014**, n/a–n/a.
29. Eda, G.; Fujita, T.; Yamaguchi, H.; Voiry, D.; Chen, M.; Chhowalla, M. Coherent Atomic and Electronic Heterostructures of Single-Layer MoS_2. *ACS Nano* **2012**, *6*, 7311–7317.
30. Wang, L.; Xu, Z.; Wang, W.; Bai, X. Atomic Mechanism of Dynamic Electrochemical Lithiation Processes of MoS_2 Nanosheets. *J. Am. Chem. Soc.* **2014**, *136*, 6693–6697.
31. Dahn, J. R. Phase-Diagram of Li_xC_6. *Phys. Rev. B* **1991**, *44*, 9170–9177.
32. Dumcenco, D. O.; Chen, K. Y.; Wang, Y. P.; Huang, Y. S.; Tiong, K. K. Raman Study of 2H-$Mo_{1-x}W_xS_2$ Layered Mixed Crystals. *J. Alloys Compd.* **2010**, *506*, 940–943.
33. Lin, F.; Nordlund, D.; Weng, T.-C.; Zhu, Y.; Ban, C.; Richards, R. M.; Xin, H. L. Phase Evolution for Conversion Reaction Electrodes in Lithium-Ion Batteries. *Nat. Commun.* **2014**, *5*, 3358–3366.
34. Seh, Z. W.; Yu, J. H.; Li, W.; Hsu, P.-C.; Wang, H.; Sun, Y.; Yao, H.; Zhang, Q.; Cui, Y. Two-Dimensional Layered Transition Metal Disulphides for Effective Encapsulation of High-Capacity Lithium Sulphide Cathodes. *Nat. Commun.* **2014**, *5*, 5017–5024.